Research Article

Muhammad Ramzan*, Ibtehal Alazman, Nazia Shahmir, and Wei Sin Koh

Analyzing the role of length and radius of MWCNTs in a nanofluid flow influenced by variable thermal conductivity and viscosity considering Marangoni convection

https://doi.org/10.1515/phys-2025-0160 received January 11, 2025; accepted May 05, 2025

Abstract: Carbon nanotubes (CNTs), formed by rolling graphene sheets into cylindrical shapes, are widely used in the development of next-generation lithium-ion batteries due to their outstanding thermal conductivity and large surface area, which enhance electrode performance, enable faster charging, and improve energy capacity. Inspired by such a fascinating application of CNTs, the present investigation examines the flow behavior of an aqueous-based nanofluid containing multi-walled carbon nanotubes (MWCNTs), utilizing the well-established Yamada-Ota thermal conductivity model to assess the influence of nanoparticle radius and length. The proposed flow model novelty lies in incorporating Marangoni convection and temperature-dependent thermophysical properties. The governing partial differential equations are transformed into ordinary differential equations through appropriate similarity transformations. Numerical solutions are obtained using the boundary value problem sol ta its ra ra CO

as extended nanotube lengths enhance heat transfer, while increased radii tend to reduce it. Additionally, Marangoni convection leads to a reduction in temperature distribution while enhancing the heat transfer rate. An increase in the variable temperature parameter results in a corresponding rise in the temperature profile. Validation of the proposed model is also included in this study.

Keywords: nanofluid flow, Yamada-Ota thermal conductivity model, energy efficiency, Marangoni convection, variable viscosity and thermal conductivity

variable thermal conductivity parameter

positive dimensional constant

constant quantities

specific heat capacity

Nomenclature

Α

 $C_{\rm p}$

Е

 C_1, C_2

solver bvp4c, with results illustrated through graphs and tables. The findings indicate that thermal conductivity reaches its peak at specific nanoparticle length $L=25\times 10^{-6}$ and radius values $R=150\times 10^{-9}$. Optimizing the length-to-radius ratio of MWCNTs in nanofluids can greatly improve thermal conductivity in high-performance electronic cooling systems	f $K_{ m NF}(T)$ L M_A m Nu Pr q_c R	dimensionless velocity variable thermal conductivity of nanofluid length of MWCNTs Marangoni parameter exponent constant Nusselt number Prandtl number heat flux radius of MWCNTs
* Corresponding author: Muhammad Ramzan, Department of Mathematics and Statistics, College of Science, Imam Mohammad Ibn Saud Islamic University (IMSIU), Riyadh, 13318, Saudi Arabia, e-mail: mramzan@bahria.edu.pk Ibtehal Alazman: Department of Mathematics and Statistics, College of Science, Imam Mohammad Ibn Saud Islamic University (IMSIU), Riyadh, 13318, Saudi Arabia Nazia Shahmir: Department of Mathematics, HITEC University, Taxila, 47080, Pakistan Wei Sin Koh: Faculty of Business and Communications, INTI International University, Persiaran Perdana BBN Putra Nilai, 71800, Nilai, Negeri Sembilan, Malaysia	S_1 T T_0 X, Y θ_R Φ σ_0 Y_T θ	nanoparticles temperature ambient temperature coordinate axis variable viscosity parameter particle volume fraction surface tension at interface temperature coefficient of surface tension dimensionless temperature density

A Open Access. © 2025 the author(s), published by De Gruyter. [This work is licensed under the Creative Commons Attribution 4.0 International License.

 $\mu_{\mathrm{NF}}(T)$ variable viscosity of nanofluid

 ψ stream function σ surface tension ζ similarity variable

 Φ_{s_1} particle volume fraction of nanoparticles

1 Introduction

Variable thermal conductivity and viscosity are crucial as they significantly influence fluid rheological properties and heat transfer performance. These characteristics are essential for designing efficient nanofluid systems used in applications like heat exchangers and renewable energy systems. Choosing variables over constant properties ensures greater accuracy for specific applications. While constant properties suffice for simple models or small temperature variations, temperature-dependent characteristics are essential for accurately modeling complex scenarios or high-temperature conditions. These variations help determine fluid flow behavior and predict actual thermal transport phenomena. Researchers increasingly emphasize the importance of temperature-dependent viscosity and thermal conductivity in advanced studies. Abu-Nada [1] conducted a groundbreaking theoretical study on nanofluid flow using an aluminum-water mixture based on the Tiwari and Das model, incorporating variable features with natural convection. Mahmoud and Megahed [2] then investigated the magnetohydrodynamic flow of a powerlaw non-Newtonian fluid film over an extended surface, considering unique variable characteristics. Subsequently, Abu-Nada et al. [3] numerically analyzed the flow of Al₂O₃-water and CuO-water nanofluid combinations in a differentially heated enclosure with variable properties. Roslan et al. [4] followed with an intriguing study using the finite difference technique to evaluate heat transfer rates in a buoyancy-driven nanofluid-filled trapezoidal enclosure under variable conditions. Sebdani et al. [5] numerically examined mixed convective nanofluid flow in a square cavity, incorporating variable viscosity and thermal conductivity. More recently, Shamshuddin and Eid [6] applied Chebyshev spectral numerical methods to study magnetized aqueous nanofluid flow with ferromagnetic nanoparticles over a stretchable spinning disk under variable features. Additional recent works exploring variable characteristics in diverse scenarios are provided in previous literature [7–10].

The Marangoni effect signifies mass transfer driven by a surface tension gradient at the interface between two liquids. When this gradient arises from temperature

differences, it is identified as thermo-capillary convection. The phenomenon was first described in 1855 by physicist James Thomson, who observed it in the "tears of wine." In this process, regions with higher surface tension pull more strongly on surrounding particles, causing the liquid to flow from areas of high to low surface tension. This gradient can result from temperature or concentration variations. The Marangoni effect has applications in crystal growth, metallurgy, soap film stabilization, Benard cells, and integrated circuit manufacturing, where it aids in drying silicon wafers. Golia and Viviani [11] introduced the concept of the Marangoni boundary layer in non-isobaric conditions, which was later explored by Montgomery and Wang [12] for a flat plate geometry. Arifin et al. [13] extended this work by studying nanoliquid flow influenced by Marangoni convection over a static flat plate using the Tiwari and Das model. Their findings showed that nanoliquids with titanium dioxide exhibited lower thermal diffusivity compared to those with copper nanoparticles. Hayat et al. [14] analytically investigated Carbon nanotube (CNT)based nanofluid flows under Marangoni convection and thermal radiative heat flux, concluding that increasing suction reduced velocity distribution for both CNTs and nanofluids. Qayyum [15] examined the Marangoni convection flow of hybrid nanoliquids in two base fluids under gravity, finding that velocity increased with the Marangoni number, while temperature decreased. Abdullah et al. [16] analyzed the electrically conducting flow of hybrid nanoliquids along a porous extending plate under Marangoni convection, observing significant temperature increases with higher magnetic parameters. Recently, Anusha et al. [17] analyzed heat and mass transfer in Marangoni convective nanofluid flow through porous media, reporting increased axial and transverse velocities with rising Marangoni numbers. Additional recent works on Marangoni convection are cited in [18–20].

A nanofluid is a combination of a conventional liquid (e.g., water or oil) and suspended nanoparticles (such as oxides, carbides, or CNTs) with sizes below 100 nm. Recognized as next-generation fluids, nanofluids exhibit superior heat transfer properties, making them invaluable for various engineering and industrial applications, including electronics, food processing, medical technologies, and energy production. Recognizing the inadequate heat transfer capabilities of conventional liquids in hightech processes, Maxwell [21] proposed the idea of mixing solid particles (particles with sizes ranging from millimeters and micrometers) with traditional liquids in 1881, to improve heat transfer capabilities. However, this concept initially faced criticism due to drawbacks such as clogging, sedimentation, and corrosion. In 1995, Choi and Eastman [22] pioneered the idea of nanofluids, updating Maxwell's theory after nearly a century. Their idea involved adding nano-sized metallic nanoparticles to conventional liquids, rather than using millimeter or micrometer-sized particles. CNTs are considered the most effective nanoparticles. Made from graphene sheet structures, CNTs are grouped as either single-walled (SWCNTs) or multi-walled (MWCNTs). SWCNTs consist of a single layer with a diameter varying from 0.5 to 1.5 nm, while MWCNTs contain interconnected tubes with progressively larger diameters. CNTs exhibit thermal, mechanical, and physicochemical properties that are six times superior, making them crucial in chemical production, optics, microelectronic cooling, and material science. Researchers have shown keen interest in exploring nanofluid flows containing CNTs over varied geometries. Yan et al. [23] experimentally studied the trend of CNTs-based hybrid non-Newtonian nanofluid flow at different temperatures. They determined that viscosity enhances for greater estimations of particle volume fraction. Harish Babu et al. [24] analyzed the inclined magnetic flux on the hybrid nanoliquid along an exponentially stretching sheet. They came to the conclusion that compared to a fundamental liquid, the temperature distribution of a hybrid nanoliquid including CNTs boosts more significantly. Next Sneha et al. [25] assessed the role of Marangoni convection and magnetic flux over the SWCNTs-based nanofluid flow in a porous media. It was shown that the rate of heat transfer was enhanced by Marangoni convection. El Glılı and Driouich [26] examined the non-orthogonal stagnation flow of CNTsnano liquid along an extending surface. Their numerical results showed that SWCNTs have a more substantial heat transmission rate compared with MWCNTs. Dero et al. [27] obtained multiple solutions of CNTs-based nanofluid flow on a permeable shrinking sheet with viscous dissipation effects. They discovered that the velocity distribution for the nanoparticles volume fraction for MWCNTs-kerosene oil is larger than that of SWCNTs-kerosene oil nanoliquid. More work on the CNTs-based nanofluid along different geometries is available in previous studies [28-31].

The reviewed literature revealed extensive studies on nanofluid flows, but only few of them have focused on Marangoni convection in such systems. Notably, none of the existing works, including those cited, provide a numerical solution for aqueous-based nanofluid flow with MWCNTs under Marangoni convection while incorporating variable thermal conductivity and viscosity. The proposed model's uniqueness lies in considering the influence of MWCNTs length and radius, analyzed using the Yamada–Ota (Y–O) thermal conductivity model. Numerical solutions are obtained through the bvp4c technique, with results presented through illustrations and tables. Table 1 highlights the novelty of the proposed model by highlighting gap analysis.

2 Mathematical formulation

The proposed mathematical model is developed based on the following assumptions:

- We consider an incompressible, aqueous-based nanofluid flow containing MWCNTs, following the Y-O thermal conductivity model.
- The Y–O thermal conductivity model is engaged to gauge the radius and length of nanoparticles in a nanofluid flow.
- The assumed nanofluid combination is in thermal balance and there is no slip between customary liquid and the assumed nanoparticles.
- Temperature-dependent thermophysical characteristics are also considered to enhance the novelty of the model.
- The flow is subjected to Marangoni convection.
- A cartesian coordinate system (x, y), where x is determined along the interface s and y is normal to it. The whole scenario is shown in Figure 1.
- Moreover, T_o is the temperature considered far off from the surface and σ is the surface tension, with expression $\sigma = \sigma_o + \left(\frac{Y_T}{2}\right)(T T_o)$, where Y_T is the temperature coefficient of surface tension [14].

Table 1: Gap analysis

Published works	Marangoni convection	Y-O thermal conductivity model	Aqueous-based nanofluid	Variable viscosity and thermal conductivity
[2]	×	×	×	\checkmark
[3]	×	×	\checkmark	\checkmark
[14]	\checkmark	×	\checkmark	×
[16]	\checkmark	×	\checkmark	×
Present	\checkmark	✓	\checkmark	\checkmark

 $[\]sqrt{\text{(Effect present)}}$, × (Effect absent).

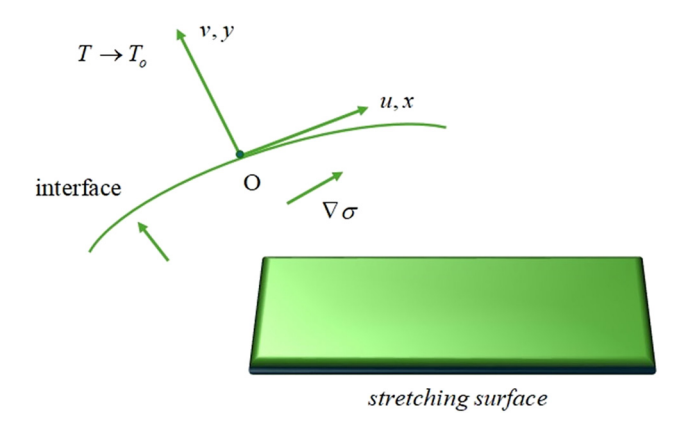


Figure 1: Geometry of the flow model.

The model equations [13] following the above assumptions are

$$\frac{\partial u}{\partial x} + \frac{\partial v}{\partial y} = 0,\tag{1}$$

$$u\frac{\partial u}{\partial x} + v\frac{\partial u}{\partial y} = \left[\frac{1}{\rho_{NF}}\right] \left[\left(\frac{\partial \mu_{NF}(T)}{\partial y}\right) \left(\frac{\partial u}{\partial y}\right) + \mu_{NF}(T) \left(\frac{\partial^{2} u}{\partial y^{2}}\right)\right], \qquad (2)$$

$$u\frac{\partial T}{\partial x} + v\frac{\partial T}{\partial y}$$

$$= \left[\frac{1}{(\rho C_{n})_{NF}}\right] \left[\left(\frac{\partial K_{NF}(T)}{\partial y}\right) \left(\frac{\partial T}{\partial y}\right) + K_{NF}(T) \left(\frac{\partial^{2} T}{\partial y^{2}}\right)\right], \qquad (3)$$

where $\mu_{NF}(T)$ is the variable viscosity given as [32]

$$\mu_{\rm NF}(T) = \mu_{\rm NF} \left(\frac{\theta_R}{\theta_R - \theta} \right),$$
 (4)

 $K_{\rm NF}(T)$ is the variable thermal conductivity and θ_R is the variable viscosity parameter, given by [32]

$$K_{\rm NF}(T) = K_{\rm NF}(1 + E\theta),\tag{5}$$

where E is the variable thermal conductivity parameter. The appropriate boundary constraints [3] are

$$\mu_{NF}(T) \left(\frac{\partial u}{\partial y} \right) = -\left(\frac{\partial \sigma}{\partial T} \right) \left(\frac{\partial T}{\partial x} \right), \quad v = 0,$$

$$T = T_w = T_0 + Ax^{m+1}, \text{ at } y = 0,$$

$$u \to 0, \quad T \to T_0, \text{ as } y \to \infty.$$
(6)

where m is the exponent constant. Similarity transformations are appended as follows:

$$\zeta = C_{2}x^{\left[\frac{m-1}{3}\right]}y, \quad \psi = C_{1}x^{\left[\frac{2+m}{3}\right]}f(\zeta),
u = C_{1}C_{2}x^{\left[\frac{2m+1}{3}\right]}f'(\zeta), \quad T = T_{0} + Ax^{m+1}\theta(\zeta),
v = -\left[C_{1}\left(\frac{2+m}{3}\right)x^{\left(\frac{m-1}{3}\right)}f(\zeta) + C_{1}x^{\left(\frac{m-1}{3}\right)}\left(\frac{m-1}{3}\right)\zeta f'(\zeta)\right].$$
(7)

By substituting Eqs. (1))–(6) in Eq. (7), we get the subsequent system

$$\left(\frac{\mu_{\rm NF}}{\rho_{\rm NF}}\right)\left(\frac{\theta_R}{\theta_R - \theta}\right)f''' + \left(\frac{\theta_R}{[\theta_R - \theta]^2}\right)\theta'f'' + \left(\frac{2+m}{3}\right)ff'' - \left(\frac{2m+1}{3}\right)f'^2 = 0,$$
(8)

$$\left(\frac{K_{\rm NF}}{(\rho C_{\rm p})_{\rm NF}}\right) (E\theta'^2 + (1 + E\theta))\theta'' - \Pr\left[(m+1)f'\theta - \left(\frac{2+m}{3}\right)f\theta'\right] = 0,$$
(9)

The constraints on the surface are outlined below

$$f(0) = 0, \quad f''(0) = -\left(\frac{\mu_{\rm NF}}{\mu_{\rm F}}\right) \left(\frac{\theta_R - \theta}{\theta_R}\right) M_A, \quad \theta(0) = 1, \quad (10)$$
$$f'(\infty) \to 0, \quad \theta(\infty) \to 0.$$

The above equations include the following dimensionless parameters:

$$M_A = \frac{AY_T(m+1)}{\mu_F C_1 C_2^2}, \text{ Pr} = \frac{\mu_f(C_p)_f}{k_f},$$
 (11)

where M_A is the Marangoni parameter and Pr is the Prandtl number. The base liquid and MWCNTs thermosphysical attributes are shown in Table 2.

2.1 Thermophysical models for nanofluid

The subsequent models are considered to reflect the thermophysical characteristics [34,35]

Dynamic viscosity

$$\mu_{\rm NF} = \mu_{\rm F}/(1 - \Phi_{\rm S1})^{2.5}$$
.

Density

$$\frac{\rho_{\rm NF}}{\rho_{\rm F}} = (1 - \Phi_{\rm s1}) + \Phi_{\rm s1} \frac{\rho_{\rm s1}}{\rho_{\rm F}}.$$

Specific heat capacity

$$\frac{(\rho C_{\rm p})_{\rm NF}}{(\rho C_{\rm p})_{\rm F}} = (1 - \Phi_{\rm S1}) + \Phi_{\rm S1} \frac{(\rho C_{\rm p})_{\rm S1}}{(\rho C_{\rm p})_{\rm F}}$$

Table 2: Thermophysical values for base fluid and nanoparticles [33]

Base fluid/nanoparticles	k	ρ	\mathcal{C}_{p}
H ₂ O	0.613	997.1	4,179
MWCNTs	3,000	1,600	796

Thermal conductivity

$$\frac{k_{NF}}{k_{F}} = \frac{1 + \frac{k_{F} L}{k_{s1} R} \Phi_{s1}^{0.2} + \left(1 - \frac{k_{F}}{k_{s1}}\right) \Phi_{s1} \frac{L}{R} \Phi_{s1}^{0.2} + 2 \Phi_{s1} \left(\frac{k_{s1}}{k_{s1} - k_{F}}\right) \ln \left(\frac{k_{s1} + k_{F}}{2k_{s1}}\right)}{1 - \Phi_{s1} + 2 \Phi_{s1} \left(\frac{k_{F}}{k_{s1} - k_{F}}\right) \ln \left(\frac{k_{s1} + k_{F}}{2k_{F}}\right)}, \tag{12}$$

where L represents the length, R is the radius of CNTs, $(k_{\rm E})$ is the thermal conductivity of fluid, (k_{s1}) is the thermal conductivity of CNTs, and (Φ_{s1}) is the particle volume fraction of CNTs.

2.2 Engineering quantity

The rate of heat flux in non-dimensional notation is given as

$$Nu = \frac{x(q_c)}{K_F(T_W - T_o)},$$

where

$$q_c = -K_{\rm NF}(T)\frac{\partial T}{\partial \nu}.$$
 (13)

The Nusselt number in dimensionless form is

$$Nu = -\left[\frac{k_{NF}}{k_{F}}(1 + E\theta)\right]C_{2}x^{\left(\frac{m+2}{3}\right)}\theta'(\zeta). \tag{14}$$

2.3 Numerical scheme

We employed the collocation technique byp4c, an efficient computational method (a finite difference mechanism) for solving sets of coupled differential equations. Using this technique, which is elaborated below, the order of the equations governing the flow is reduced to one. A technique to transform the higher-order system to one is appended as under

$$y_{1} \to f, \quad y_{2} \to f', \quad y_{3} \to f'', \quad yy_{1} \to f''',$$

$$y_{4} \to \theta, \quad y_{5} \to \theta', \quad yy_{2} \to \theta'',$$

$$yy_{1} = \left[\frac{1}{\left(\frac{\mu_{NF}}{\rho_{NF}}\right)\left(\frac{\theta_{R}}{\theta_{R} - y_{4}}\right)}\right] \left[-\left(\frac{\theta_{R}}{[\theta_{R} - y_{4}]^{2}}\right)y_{5}y_{3} - \left(\frac{2 + m}{3}\right)y_{1}y_{3}\right]$$

$$+ \left(\frac{2m + 1}{3}\right)(y_{2})^{2},$$

$$yy_{2} = \left[\frac{1}{\left(\frac{K_{NF}}{(\rho C_{p})_{NF}}\right)(Ey_{5}^{2} + (1 + Ey_{4}))}\right] \Pr\left[(m + 1)y_{2}y_{4}\right]$$

$$- \left(\frac{2 + m}{3}\right)y_{1}y_{5},$$

$$y_{1}(0), \quad y_{3}(0) + \left(\frac{\mu_{NF}}{\mu_{F}}\right)\left(\frac{\theta_{R} - y_{4}}{\theta_{R}}\right)M_{A}, \quad y_{4}(0) - 1, \quad (15)$$

$$y_1(0), \ y_3(0) + \left(\frac{\mu_{NF}}{\mu_F}\right) \left(\frac{\theta_R - y_4}{\theta_R}\right) M_A, \ y_4(0) - 1,$$
 (15)
 $y_2(\infty) \to 0, \ y_4(\infty) \to 0.$

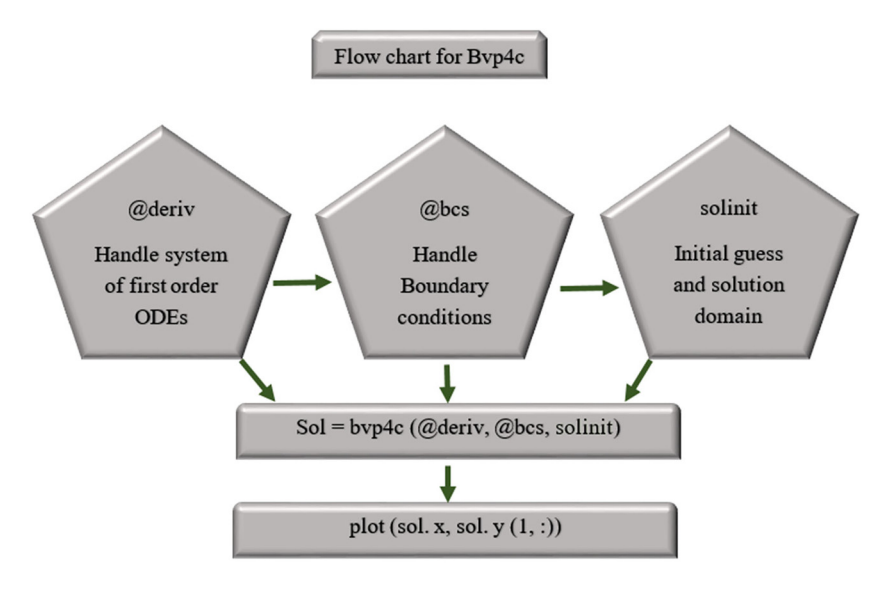


Figure 2: Flow chart of bvp4c numerical scheme.

A step size of $\Delta \eta = 0.01$ with $\eta_{\infty} = 14$ is considered for all profiles for convergence purposes. Another important ingredient of this numerical scheme is the consideration of the initial guess that must satisfy the assumed boundary conditions. A complete flow diagram of the numerical technique (bvp4c) is given in Figure 2.

This technique possesses the following advantages over the contemporary analytical and numerical schemes:

- The bvp4c automatically adapts the mesh size for enhanced accuracy. By doing so we can achieve accuracy without user interference.
- In comparison to the traditional techniques, bvp4c efficiently handles the discontinuities.
- Contrary to analytical techniques, it handles nonlinear boundary value problems effectively.
- The bvp4c is simpler and straightforward to implement with less effort.
- In comparison to finite difference, the bvp4c method engages the collocation method leading to higher accuracy.

Table 3 portrays the numerical results of heat transmission rate for different estimations of variable thermal conductivity parameter (E), Marangoni parameter (M_A) , and exponent constant (m). It is noted that the heat transmission rate improves for mounting estimations of all three parameters. This is because the improved values of variable thermal conductivity parameter result in enhanced diffusion that eventually triggers the heat transfer rate. Similarly, stronger thermocapillary convection is observed for increased Marangoni parameter that improves the fluid movement at the surface. Thus, enhanced heat transfer efficacy at the fluid interface is seen. Likewise, a large value of exponent triggers the thermal conductivity in high temperatures that eventually leads to an efficient heat transfer rate.

 $\begin{tabular}{ll} \textbf{Table 3:} Numerical estimates of Nusselt number Nu against varied parameters \\ \end{tabular}$

(E)	(<i>M</i> _A)	(m)	(Nu)
0.1	0.10	0.1	0.84463
0.2			0.90408
0.3			0.95993
0.4			1.01320
	0.12 0.13		0.89717
			0.92157
	0.14		0.94454
		0.2	0.86797
		0.3	0.89031
		0.4	0.91179

Table 4: Numerical estimates of thermal conductivity against higher values of particle volume fraction

$oldsymbol{\Phi}_{ m NF}$	$k_{ m NF}$
0.01	1.344517154332972
0.02	1.830524151848501
0.03	2.498053161467530
0.04	3.440034976804251
0.05	4.841142856090153
0.06	7.111676268043935

The variation in thermal conductivity with particle volume fractions ranging from 1 to 6% is shown in Table 4, with the MCNTs length held constant. As the particle volume fraction of MCNTs increases at a fixed length, thermal conductivity is observed to rise. This finding aligns well with the experimental results stated by Assael et al. [35].

3 Graphical results analysis

This section aims to inspect the consequences of emerging factors on various flow and thermal distributions.

From Figure 3, the impact of length (L) of MWCNTs on the thermal conductivity can be observed. It is seen that for raising the length of MWCNTs, the thermal conductivity of nanofluid flow is significantly enhanced. This enhancement in the thermal conductivity may be owing to the high intrinsic thermal conductivity of MWCNTs, their aspect ratio, and uniform dispersion of MWCNTs in water, and volume fraction.

The role of the radius (R) of MWCNTs over the thermal conductivity can be visualized in Figure 4. It is inferred that for improving the radius of MWCNTs, the thermal

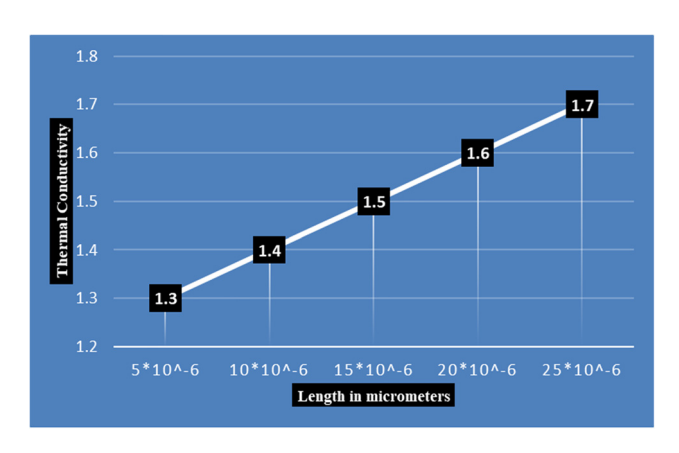


Figure 3: Upshot of length of MWCNTs on the thermal conductivity $K_{\rm NF}$.

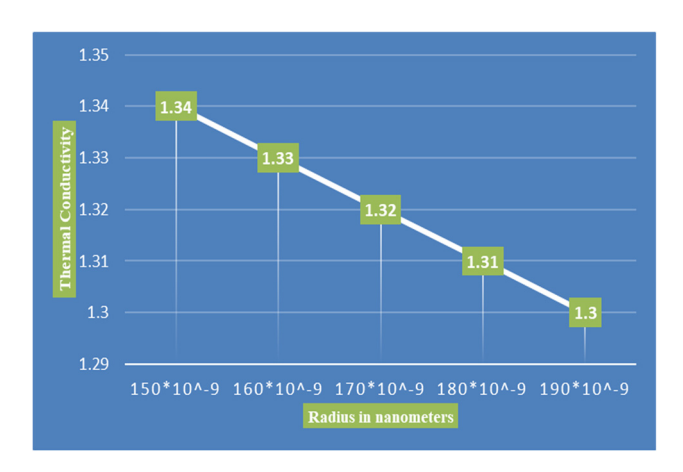


Figure 4: Upshot of radius of MWCNTs on the thermal conductivity $K_{\rm NF}$.

conductivity drops. Here the factors affecting thermal conductivity may include increased inter-layer scattering, thermal boundary resistance, and contact resistance in composites.

The role of the Marangoni parameter (M_A) on the velocity distribution $f'(\zeta)$ can be seen in Figure 5 . It is seen that velocity distribution escalates for mounting values of (M_A) . Marangoni convection causes the fluid to flow at higher velocities in areas with a noticeable surface tension noted. When there are significant temperature differences close to borders or interfaces, this impact may be very noticeable.

The trend of velocity distribution $f'(\zeta)$ against the particle volume fraction (Φ) , is shown in Figure 6. It is seen that raising counts of particle volume fraction (Φ) upsurges the velocity distribution. Physically, strengthening the particle volume fraction causes a rapid collision of nanoparticles, which improves the velocity distribution.

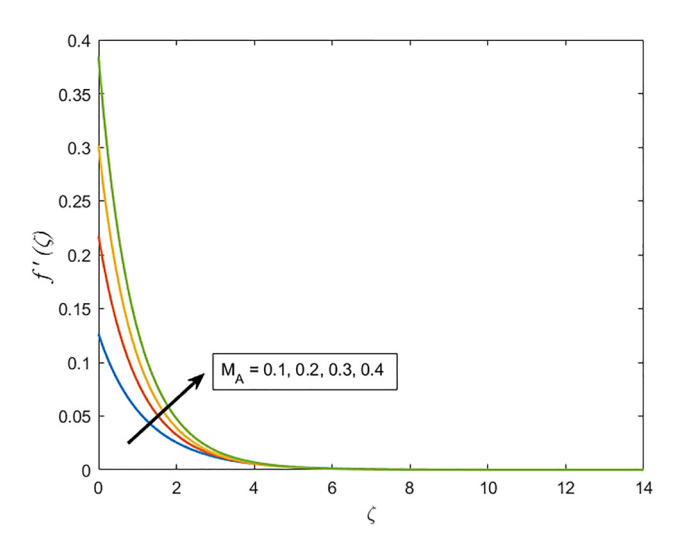


Figure 5: Upshot of Marangoni parameter (M_A) on $f'(\zeta)$.

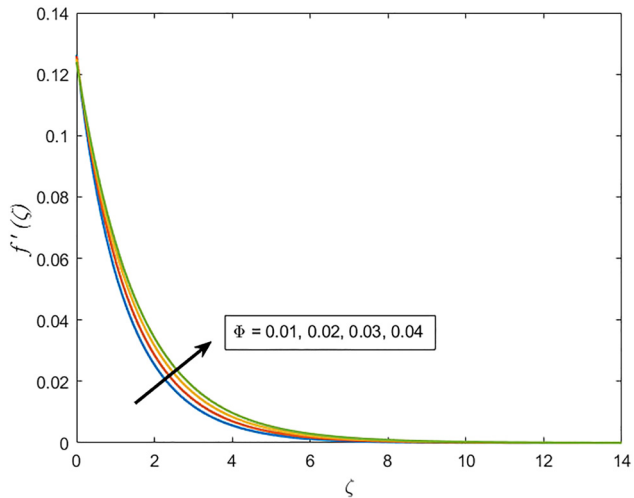


Figure 6: Upshot of particle volume fraction (Φ) on $f'(\zeta)$.

Figure 7 reveals the impact of the variable viscosity parameter (θ_R) on the velocity distribution $f'(\zeta)$. It is seen that velocity distribution escalates by greater values of (θ_R) . This is due to the fact that rising (θ_R) implies zero shear rate viscosity, which lowers viscous drag force and speeds up flow.

The influence of the exponent constant (m) on the velocity distribution $f'(\zeta)$ is displayed in Figure 8. It is seen that velocity distribution drops significantly for greater counts of (m). When m rises, the temperature variation throughout the surface reduces, resulting in a lesser velocity distribution.

Figure 9 is portrayed to analyze the consequences of the Marangoni parameter (M_A) on the temperature distribution $\theta(\zeta)$. It is seen that temperature distribution dwindled for the greater counts of (M_A) . The higher estimates of (M_A) enhance the surface tension resulting in

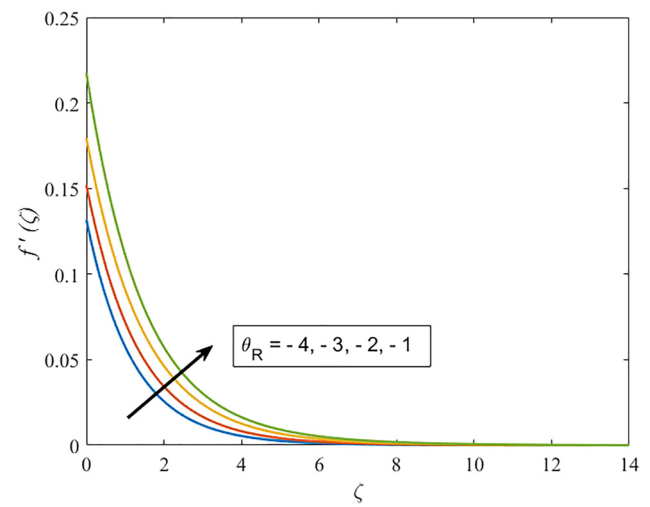


Figure 7: Upshot of variable viscosity parameter (θ_R) on $f'(\zeta)$.

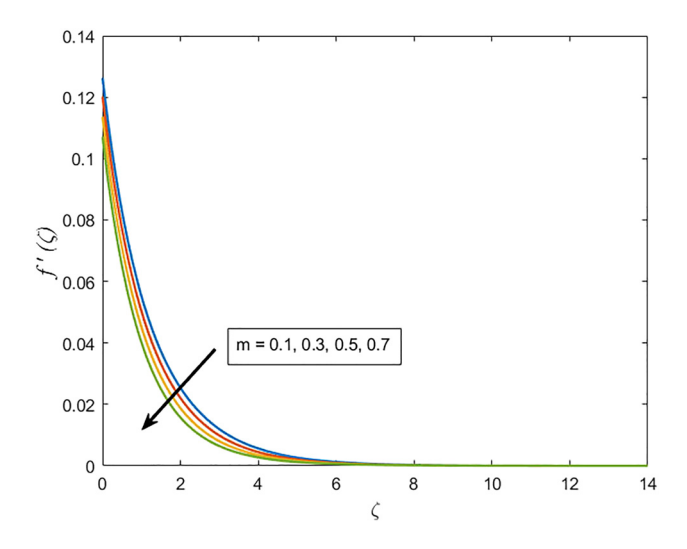


Figure 8: Upshot of exponent constant (m) on $f'(\zeta)$.

improved heat transfer, thus reducing the temperature gradient with the assumed fluid flow.

The role of particle volume fraction (Φ) on the temperature distribution is displayed in Figure 10. It is revealed that the temperature distribution of nanofluid containing MWCNTs nanoparticles escalates for mounting (Φ) . Adding more MWCNTs nanoparticles to the fluid enhances heat transfer capabilities owing to the high thermal conductivity of MWCNTs. This results in an improved heat transfer rate.

Finally, the role of variable thermal conductivity (E) on the temperature distribution can be analyzed from Figure 11. It is revealed that temperature distribution escalates for greater counts of (E). This is because the temperature is increased as a consequence of the quicker heat transfer process from sheet to fluid.

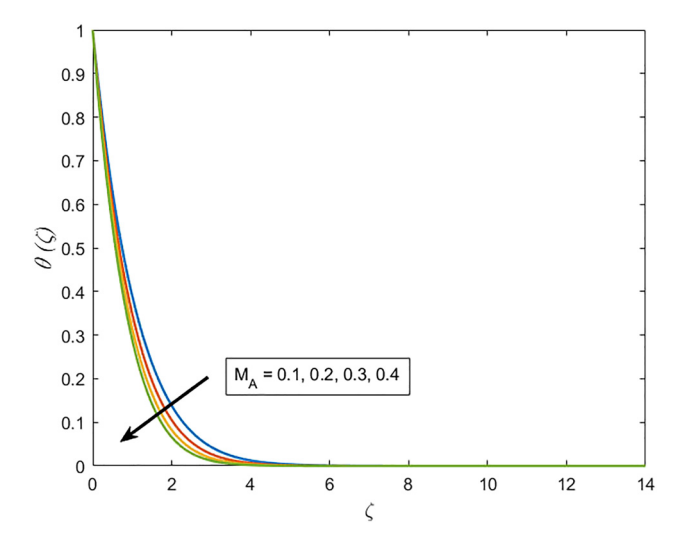


Figure 9: Upshot of Marangoni parameter (M_A) on $\theta(\zeta)$.

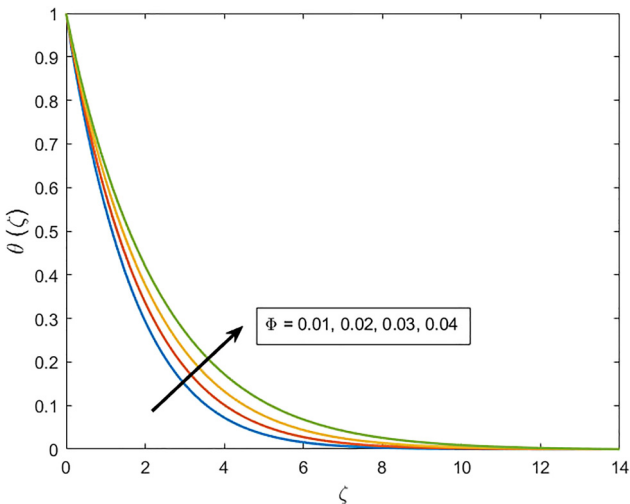


Figure 10: Upshot of particle volume fraction (Φ) on $\theta(\zeta)$.

To validate the outcomes of the proposed mode, a comparison with Montgomery and Wang [12] when m=0 is made. An excellent correlation is achieved (Figure 12).

4 Conclusion

This study examined the thermal properties of aqueous nanofluid flow containing immersed MWCNTs influenced by Marangoni convection. Temperature-dependent models for viscosity and thermal conductivity were utilized instead of constant values. The Y–O model was applied to analyze the impact of radius and length on nanofluid thermal

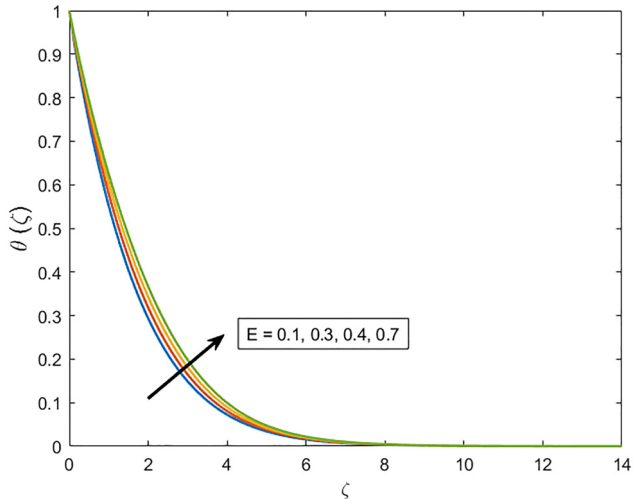


Figure 11: Upshot of variable thermal conductivity (E) on $\theta(\zeta)$.

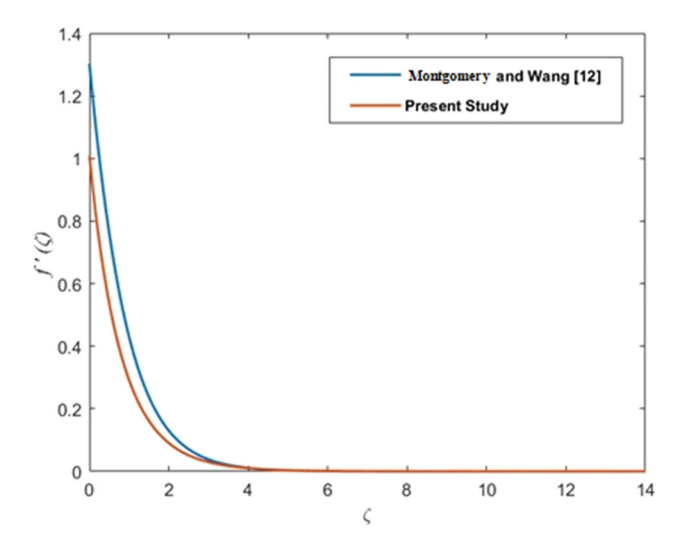


Figure 12: Comparison with published work [12] when m = 0.

conductivity. Numerical results were obtained using the bvp4c method. Key findings are summarized below:

- · Increasing the length of MWCNTs improves the nanofluid's thermal conductivity, whereas increasing the radius reduces it.
- The thermal conductivity is improved in order to increase the particle volume fraction while maintaining the fixed length of MWCNTs.
- · The Marangoni parameter boosts the velocity distribution while diminishing the temperature distribution.
- Velocity distribution escalates by raising the viscosity parameter and particle volume fraction.
- It is seen that velocity distribution drops significantly for greater counts of exponent constant.
- By raising the variable temperature parameter, the temperature distribution escalates.
- Marangoni convection drops the temperature distribution but enhances the heat transmission rate.

Acknowledgments: This work was supported and funded by the Deanship of Scientific Research at Imam Mohammad Ibn Saud Islamic University (IMSIU) (grant number IMSIU-DDRSP2503).

Funding information: This work was supported and funded by the Deanship of Scientific Research at Imam Mohammad Ibn Saud Islamic University (IMSIU) (grant number IMSIU-DDRSP2503).

Author contributions: All authors have accepted responsibility for the entire content of this manuscript and approved its submission.

Conflict of interest: The authors state no conflict of interest.

Data availability statement: Data sharing is not applicable to this article as no datasets were generated or analyzed during the current study.

References

- Abu-Nada E. Effects of variable viscosity and thermal conductivity of Al₂O₃-water nanofluid on heat transfer enhancement in natural convection. Int J Heat Fluid Flow. 2009;30(4):679-90. doi: 10.1016/j. iiheatfluidflow.2009.02.003.
- Mahmoud MA, Megahed AM. MHD flow and heat transfer in a non-[2] Newtonian liquid film over an unsteady stretching sheet with variable fluid properties. Can J Phys. 2009;87(10):1065-71. doi: 10. 1139/P09-066.
- Abu-Nada E, Masoud Z, Oztop HF, Campo A. Effect of nanofluid [3] variable properties on natural convection in enclosures. Int J Therm Sci. 2010;49(3):479-91. doi: 10.1016/j.ijthermalsci.2009.09.002.
- [4] Roslan R, Saleh H, Hashim I. Buoyancy-driven heat transfer in nanofluid-filled trapezoidal enclosure with variable thermal conductivity and viscosity. Numer Heat Transfer, Part A: Appl. 2011;60(10):867-82. doi: 10.1080/10407782.2011.616778.
- [5] Sebdani SM, Mahmoodi M, Hashemi SM. Effect of nanofluid variable properties on mixed convection in a square cavity. Int J Therm Sci. 2012;52:112-26. doi: 10.1016/j.ijthermalsci.2011.09.003.
- Shamshuddin MD, Eid MR. Magnetized nanofluid flow of [6] ferromagnetic nanoparticles from parallel stretchable rotating disk with variable viscosity and thermal conductivity. Chin J Phys. 2021;74:20-37. doi: 10.1016/j.cjph.2021.07.038.
- Alharbi KAM, Shahmir N, Ramzan M, Almusawa MY, Kadry S. Bioconvective radiative unsteady Casson nanofluid flow across two concentric stretching cylinders with variable viscosity and variable thermal conductivity. Numer Heat Transfer, Part A: Appl. 2024;85(10):1653-70. doi: 10.1080/10407782.2023.2208733.
- [8] Mandal G, Pal D. Dual solutions of radiative Aq-MoS₂/water hybrid nanofluid flow with variable viscosity and variable thermal conductivity along an exponentially shrinking permeable Riga surface: Stability and entropy generation analysis. Int J Model Simul. 2023;44(6):360-85. doi: 10.1080/02286203.2023.2171656.
- [9] Govindarajulu K, Subramanyam Reddy A, Jagadeshkumar K, Srinivas S, Kumar BR, Vajravelu K. Entropy generation on MHD pulsatile flow of third grade hybrid nanofluid in a vertical porous channel with nonuniform heat source/sink, variable viscosity, thermal conductivity, and Joule heating: a numerical study. Numer Heat Transfer, Part A: Appl. 2023;85(24):4184-203. doi: 10.1080/10407782.2023.2255929.
- Babu MS, Sankar GR, Velpula VR, Chu YM, Khan MI, Raju CSK, et al. Chemically reactive flow of viscous thermophoretic fluid over wedge with variable thermal conductivity and viscosity. Case Stud Therm Eng. 2023;45:102924. doi: 10.1016/j.csite.2023.102924.
- Golia C, Viviani A. Non isobaric boundary layers related to Marangoni flows. Meccanica. 1986;21:200-4.
- [12] Montgomery CD, Wang B. Prandtl number effects for Marangoni convection over a flat surface. Int J Therm Sci. 2001;40(6):564-70. doi: 10.1016/S1290-0729(01)01244-3.
- [13] Arifin NM, Nazar R, Pop I. Similarity solution of Marangoni convection boundary layer flow over a flat surface in a nanofluid. | Appl Math. 2013;2013:634746. doi: 10.1155/2013/634746.

- [14] Hayat T, Khan MI, Farooq M, Alsaedi A, Yasmeen T. Impact of Marangoni convection in the flow of carbon–water nanofluid with thermal radiation. Int J Heat Mass Transf. 2017;106:810–5. doi: 10. 1016/j.ijheatmasstransfer.2016.08.115.
- [15] Qayyum S. Dynamics of Marangoni convection in hybrid nanofluid flow submerged in ethylene glycol and water base fluids. Int Commun Heat Mass Transfer. 2020;119:104962. doi: 10.1016/j. icheatmasstransfer.2020.104962.
- [16] Abdullah NN, Som ANM, Arifin NM, Ab Ghani A. The effect of MHD on Marangoni boundary layer of hybrid nanofluid flow past a permeable stretching surface. CFD Letters. 2023;15(5):65–73. doi: 10.37934/cfdl.15.5.6573.
- [17] Anusha T, Pérez LM, Mahabaleshwar US, Zeidan D. An MHD nanofluid flow with Marangoni laminar boundary layer over a porous medium with heat and mass transfer. Int J Model Simul. 2024;1–17. doi: 10.1080/02286203.2024.2335112.
- [18] Abbas M, Khan N, Hashmi MS, Alhefthi RK, Rezapour S, Inc M. Thermal Marangoni convection in two-phase quadratic convective flow of dusty MHD trihybrid nanofluid with non-linear heat source. Case Stud Therm Eng. 2024;57:104190. doi: 10.1016/j.csite.2024.104190.
- [19] Abbas M, Khan N, Shehzad SA. Numerical analysis of Marangoni convected dusty second-grade nanofluid flow in a suspension of chemically reactive microorganisms. Proc Inst Mech Eng, Part C-J Mech Eng Sci. 2024;238(10):4400–17. doi: 10.1177/09544062231209828.
- [20] Rehman A, Khun MC, Alsubaie AS, Inc M. Influence of Marangoni convection, viscous dissipation, and variable fluid viscosity of nanofluid flow on stretching surface analytical analysis. ZAMM - J Appl Math Mech. 2024;104(3):e202300413. doi: 10.1002/zamm. 202300413.
- [21] Maxwell JC. A treatise on electricity and magnetism. Vol. 1, Oxford: Clarendon Press; 1873.
- [22] Choi SU, Eastman JA. Enhancing thermal conductivity of fluids with nanoparticles. San Francisco, USA: ASME International Mechanical Engineering Congress & Exposition; 1995.
- [23] Yan SR, Toghraie D, Abdulkareem LA, Alizadeh AA, Barnoon P, Afrand M. The rheological behavior of MWCNTs–ZnO/Water–Ethylene glycol hybrid non-Newtonian nanofluid by using of an experimental investigation. J Mater Res Technol. 2020;9(4):8401–6.
- [24] Harish Babu D, Naidu KK, Deo S, Satya Narayana PV. Impacts of inclined Lorentz forces on hybrid CNTs over an exponentially stretching sheet with slip flow. Int J Model Simul. 2023;43(3):310–24. doi: 10.1080/02286203.2022.2079109.
- [25] Sneha KN, Bognar G, Mahabaleshwar US, Singh DK, Singh OP. Magnetohydrodynamics effect of Marangoni nano boundary layer flow and heat transfer with CNT and radiation. J Magn Magn Mater. 2023;575:170721. doi: 10.1016/j.jmmm.2023.170721.

- [26] El Glili I, Driouich M. Impact of inclined magnetic field on non-orthogonal stagnation point flow of CNT-water through stretching surface in a porous medium. J Therm Eng. 2024;10(1):115–29. doi: 10.18186/thermal.1429409.
- [27] Dero S, Fadhel MA, Lund LA, Shah NA. Multiple solutions of unsteady flow of CNTs nanofluid over permeable shrinking surface with effects of dissipation and slip conditions. Mod Phys Lett B. 2024;38(15):2450120. doi: 10.1142/S0217984924501203.
- [28] Bakhtiyar NK, Esmaeili S, Javadpour R, Heris SZ. Experimental investigation of indirect heat transfer through a novel designed lab-scale setup using functionalized MWCNTs nanofluids (MWCNTs-COOH/water and MWCNTs-OH/water). Case Stud Therm Eng. 2023;45:102951. doi: 10.1016/j.csite.2023.102951.
- [29] Pourpasha H, Heris SZ, Mousavi SB. Thermal performance of novel ZnFe₂O₄ and TiO₂-doped MWCNT nanocomposites in transformer oil. J Mol Liq. 2024;394:123727. doi: 10.1016/j.molliq.2023.123727.
- [30] Farooq U, Liu T, Farooq U, Majeed S. Non-similar analysis of bioconvection MHD micropolar nanofluid on a stretching sheet with the influences of Soret and Dufour effects. Appl Water Sci. 2024;14(6):116. doi: 10.1007/s13201-024-02143-0.
- [31] Liu Z, Ali AB, Hussein RA, Singh NSS, Al-Bahrani M, Abdullaeva B, et al. Using evolutionary algorithms and group method of data handling ANN for prediction of the viscosity MWCNT-ZnO/oil SAE 50 nano-lubricant. Int Commun Heat Mass Transf. 2025;163:108749. doi: 10.1016/j.icheatmasstransfer.2025.108749.
- [32] Swain K, Parida SK, Dash GC. MHD heat and mass transfer on stretching sheet with variable fluid properties in porous medium. AMSE J Model B. 2017;86:706–26.
- [33] Muhammad S, Ali G, Shah Z, Islam S, Hussain SA. The rotating flow of magneto hydrodynamic carbon nanotubes over a stretching sheet with the impact of non-linear thermal radiation and heat generation/absorption. Appl Sci. 2018;8(4):482. doi: 10.3390/ app8040482.
- [34] Khashi'ie NS, Arifin NM, Hafidzuddin EH, Wahi N, Pop I. Mixed convective stagnation point flow of a thermally stratified hybrid Cu-Al₂O₃/water nanofluid over a permeable stretching/shrinking sheet. ASM Sci J Akademi Sains Malays. 2019;12:17–25. doi: 10. 1038/s41598-023-34686-8. for ICoAIMS2019; Alharbi KAM, Ramzan M, Shahmir N, Ghazwani HAS, Elmasry Y, Eldin SM, et al. Comparative appraisal of mono and hybrid nanofluid flows comprising carbon nanotubes over a three-dimensional surface impacted by Cattaneo-Christov heat flux. Sci Report. 2023;13(1):7964.
- [35] Assael MJ, Chen CF, Metaxa I, Wakeham, WA. Thermal conductivity of suspensions of carbon nanotubes in water. Int J Thermophys. 2004;25:971–85. doi: 10.1023/B:IJOT.0000038494.22494.04.

Appendix

$$\begin{split} \frac{\partial u}{\partial x} &= C_1 C_2 \bigg(\frac{2m+1}{3}\bigg) x^{\frac{2m-2}{3}} f' + C_1 C_2 \zeta \bigg(\frac{m-1}{3}\bigg) x^{\frac{2m-2}{3}} f'', \\ \frac{\partial v}{\partial y} &= -C_1 C_2 \bigg(\frac{2m+1}{3}\bigg) x^{\frac{2m-2}{3}} f' - C_1 C_2 \zeta \bigg(\frac{m-1}{3}\bigg) x^{\frac{2m-2}{3}} f'', \\ \frac{\partial u}{\partial y} &= C_1 C_2^2 x^m f'', \\ \frac{\partial^2 u}{\partial y^2} &= C_1 C_2^3 x^{\frac{4m-1}{3}} f''', \\ \frac{\partial T}{\partial x} &= A(m+1) x^m \theta + A x^m \zeta \theta', \\ \frac{\partial T}{\partial y} &= A C_2 x^{\frac{4m+2}{3}} \theta', \end{split}$$

$$\frac{\partial^2 T}{\partial y^2} = AC_2^2 x^{\frac{3m-1}{3}} \theta'',$$

$$\frac{\partial \mu_{\rm NF}(T)}{\partial y} = \mu_{\rm NF} \left(\frac{\theta_R}{(\theta_R - \theta)^2} \right) C_2 x^{\frac{m-1}{3}} \theta',$$

$$\frac{\partial K_{\rm NF}(T)}{\partial y} = K_{\rm NF} EC_2 x^{\frac{m-1}{3}} \theta'. \tag{A1}$$

Using the above values of partial derivative in model equations, the set of reduced differential equations will be obtained.